

ARTICLE



Mechanosensitive turnover of phosphoribosyl pyrophosphate synthetases regulates nucleotide metabolism

Jingyi Li^{1,2,6}, Jichun Shao^{1,6}, Zhijun Zeng^{1,6}, Yumin He³, Can Tang², Su Hwan Park⁴, Jong-Ho Lee^{4,5} and Rui Liu³✉

© The Author(s), under exclusive licence to ADMC Associazione Differenziamento e Morte Cellulare 2021

Cells coordinate their behaviors with the mechanical properties of the extracellular matrix (ECM). Tumor cells frequently harbor an enhanced nucleotide synthesis, presumably to meet the increased demands for rapid proliferation. Nevertheless, how ECM rigidity regulates nucleotide metabolism remains elusive. Here we show that shift from stiff to soft matrix blunts glycolysis-derived nucleotide synthesis in tumor cells. Soft ECM results in TNF receptor-associated factor 2 (TRAF2)-dependent K29 ubiquitination and degradation of phosphoribosyl pyrophosphate synthetase (PRPS)1/2. Recruitment of TRAF2 to PRPS1/2 requires phosphorylation of PRPS1 S285 or PRPS2 T285, which is mediated by low stiffness-activated large tumor suppressor (LATS)1/2 kinases. Further, non-phosphorylatable or non-ubiquitinatable PRPS1/2 mutations maintain PRPS1/2 expression and nucleotide synthesis at low stiffness, and promote tumor growth and metastasis. Our findings demonstrate that PRPS1/2 stability and nucleotide metabolism is ECM rigidity-sensitive, and thereby highlight a regulatory cascade underlying mechanics-guided tumor metabolism reprogramming.

Cell Death & Differentiation (2022) 29:206–217; <https://doi.org/10.1038/s41418-021-00851-7>

INTRODUCTION

Solid tumors are characterized by an abnormally developed stroma that endows the tumor environment with an increased extracellular matrix (ECM) rigidity [1]. ECM rigidity, varying with its composition and organization, depicts the capacity to which a material resists deformation upon exerted forces. The mechanical signals that tumor cells sense during interaction with the surroundings dictate a wide spectrum of cellular processes, such as filopodia formation and extension, and are evidenced to modulate tumor progression [2]. However, the key factors involved in mechanotransduction during cell-matrix interplay remain elusive.

Nucleotide metabolism provides building blocks for DNA and RNA synthesis to support the rapid proliferation of tumor cells. The five-carbon ribose of nucleotides originates from glycolysis. Pentose phosphate pathway (PPP), an alternative branch of glycolysis, utilizes glycolytic intermediates glucose-6-phosphate and fructose-6-phosphate to produce ribose-5-phosphate (R5P) and subsequent phosphoribosyl pyrophosphate (PRPP), which is prerequisite in both de novo and salvage pathways to yield nucleotides [3] (Fig. S1A). Conversion of R5P to PRPP, where the β - and γ -diphosphoryl moieties of adenosine triphosphate (ATP) were transferred onto the C1-hydroxy group of R5P, is governed by a group of phosphoribosyl pyrophosphate synthetases (PRPSs) [4] and is the rate-limiting step for nucleotide synthesis. In total, mammals have three distinct PRPS genes, whose coding products share high similarities with each other. Among them,

expression of PRPS1 and PRPS2 is detected in a variety of organs, while expression of PRPS3 is testis-specific [5]. However, whether nucleotide metabolism is regulated in response to ECM rigidity is largely unknown.

In this study, we demonstrate that large tumor suppressor kinase (LATS)1/2 phosphorylate PRPS1 S285 and PRPS2 T285 at low stiffness, which in turn results in PRPS1/2 K29 ubiquitination and degradation in an E3 ligase TRAF2-dependent manner. Stabilization of PRPS1/2 restores low stiffness-repressed nucleotide synthesis and accelerates tumorigenesis.

RESULTS**Low stiffness dampens nucleotide synthesis and PRPS1/2 expression**

To examine the impact of matrix rigidity on the regulation of nucleotide synthesis, human colorectal cancer HCT116 cells, prostate cancer DU145 cells, and oral squamous cell carcinoma HSC-3 cells were cultured on stiff (40.19 ± 3.19 kPa, referred to 40 kPa) or soft (0.98 ± 0.029 kPa, referred to 1 kPa) polyacrylamide (PAAm)-based matrix [6, 7], which caused palpable changes in the GTP-bound form of RhoA, ROCK1/2 activity and phosphorylation of MYPT1 T696 [8] (Fig. S1B). After incubation with [¹⁴C]-glucose (0.01 mmol/L), we found an apparently lowered production of radioactive DNA and RNA in those cells cultured at 1 kPa (Figs. 1A and S1C). A more pronounced decrease was observed in comparison with the cells cultured on basement membrane-

¹The Second Affiliated Hospital of Chengdu Medical College, China National Nuclear Corporation 416 Hospital, Chengdu, China. ²School of Biological Sciences and Technology, Chengdu Medical College, Chengdu, China. ³State Key Laboratory of Oral Diseases, National Clinical Research Center for Oral Diseases, Chinese Academy of Medical Sciences Research Unit of Oral Carcinogenesis and Management, West China Hospital of Stomatology, Sichuan University, Chengdu, China. ⁴Department of Health Sciences, The Graduate School of Dong-A University, Busan, Republic of Korea. ⁵Department of Biological Sciences, Dong-A University, Busan, Republic of Korea. ⁶These authors contributed equally: Jingyi Li, Jichun Shao, Zhijun Zeng. ✉email: liurui_scu@hotmail.com
Edited by C. Borner

Received: 17 December 2020 Revised: 2 August 2021 Accepted: 5 August 2021

Published online: 31 August 2021

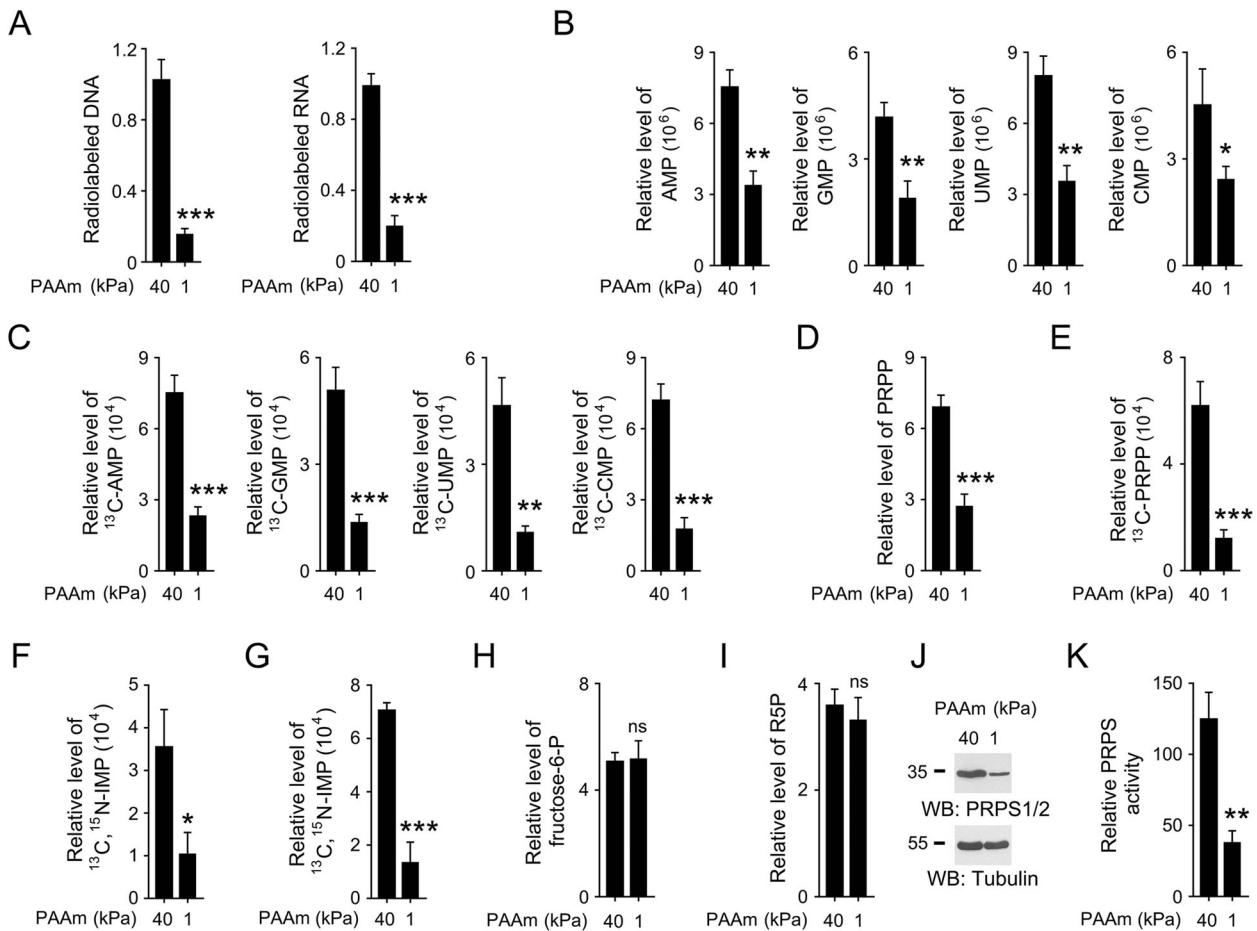


Fig. 1 Low stiffness dampened nucleotide synthesis and PRPS1/2 expression. **A–K** Cells were cultured on a stiff (40 kPa) or soft (1 kPa) matrix for 24 h before the indicated measurement or treatment. **A–I, K** Data represent the mean and SD from three independent experiments. * $P < 0.05$; ** $P < 0.01$; *** $P < 0.001$; ns, not significant. **A** HCT116 cells were labeled with $^{14}\text{C}_6$ -glucose (1 μCi , 0.01 mmol/L) for 2 h, and the amounts of ^{14}C -DNA and ^{14}C -RNA were measured. **B, D, H, I** Indicated metabolites in HCT116 cells were measured. **C, E** HCT116 cells were labeled with $^{13}\text{C}_6$ -glucose (10 mmol/L) for 2 h, and the indicated ^{13}C -labeled metabolites were measured. **F, G** HCT116 cells were labeled with [$^{13}\text{C}_2, ^{15}\text{N}$]-glycine (0.4 mmol/L, **F**) or [$^{13}\text{C}_5, ^{15}\text{N}_4$]-hypoxanthine (0.1 mmol/L, **G**) for 2 h, and the levels of labeled IMP were measured. **J** Expression of PRPS1/2 was measured by immunoblot. The anti-PRPS1/2 antibody recognizes both PRPS1 and PRPS2. **K** PRPS activities in HCT116 cell lysates were measured.

coated plastics (Fig. S1D, E). Consistently, soft matrix decreased the cellular level of either purine and pyrimidine intermediates (Figs. 1B and S1F), as well as the conversion of [^{13}C]-glucose to these intermediates (Figs. 1C and S1G). Notably, both steady level and synthesis of PRPP were reduced at low stiffness (Figs. 1D, E and S1H, I). To determine the effects on the de novo and salvage pathways, both of which utilize PRPP as a substrate, HCT116 cells were labeled with [$^{13}\text{C}_2, ^{15}\text{N}$]-glycine or [$^{13}\text{C}_5, ^{15}\text{N}_4$]-hypoxanthine, respectively. Indeed, the level of glycine or hypoxanthine-derived inosine monophosphate (IMP), a purine intermediate, was substantially declined in response to low matrix rigidity, indicating a reduction in both pathways (Fig. 1F, G). Nevertheless, no palpable differences were found in the level of fructose-6-P or R5P in HCT116, DU145 or HSC-3 cells (Figs. 1H, I and S1J, K), suggesting that the altered nucleotide synthesis was not likely due to the changes in glycolysis or PPP pathway.

Production of PRPP from R5P is governed by PRPSs [4]. Separate knockdown of PRPS1 or PRPS2 caused about 25–65% reduction in cellular PRPS activity in HCT116, DU145, or HSC-3 cells (Fig. S1L, M). Strikingly, the culture of these cells on the soft matrix resulted in a considerable decrease in PRPS1/2 expression, shown by immunoblot analyses (Figs. 1J, S1N, and S1O). Accordingly, PRPS activity in cell lysates was conformably decreased (Fig. 1K, S1N,

and S1O). These results suggest that low stiffness dampens nucleotide synthesis and PRPS1/2 expression.

TRAF2 mediates poly-ubiquitination and degradation of PRPS1/2 at low stiffness

We next tested whether PRPS1/2 gene transcription was altered in response to ECM rigidity. However, reverse transcription-polymerase chain reaction (RT-PCR) analysis revealed comparable PRPS1/2 mRNA levels (Fig. S2A). To determine whether PRPS1/2 protein stability was altered, we treated HCT116 cells with cycloheximide (CHX) to block protein synthesis. Normalization of the immunoblot signals revealed that culture on soft matrix largely shortened the half-life of PRPS1/2 protein (Figs. 2A and S2B). Further, soft matrix-repressed PRPS1/2 expression could be restored by treatment with proteasome inhibitor MG132, hinting at the possible involvement of proteasome-dependent protein degradation (Fig. S2C). Indeed, soft matrix enhanced a high molecular weight smear of the ubiquitinated PRPS1/2 (Fig. S2D). Of note, this ubiquitination was abrogated by expression of an HA-ubiquitin lysine (K)48arginine (R) mutant, but not K63R mutant (Fig. S2D), which prevents poly-ubiquitin chain formation by intermolecular cross-linking at K48 or K63, respectively. These data suggest that matrix rigidity regulates PRPS1/2 stability through K48-dependent ubiquitylation.

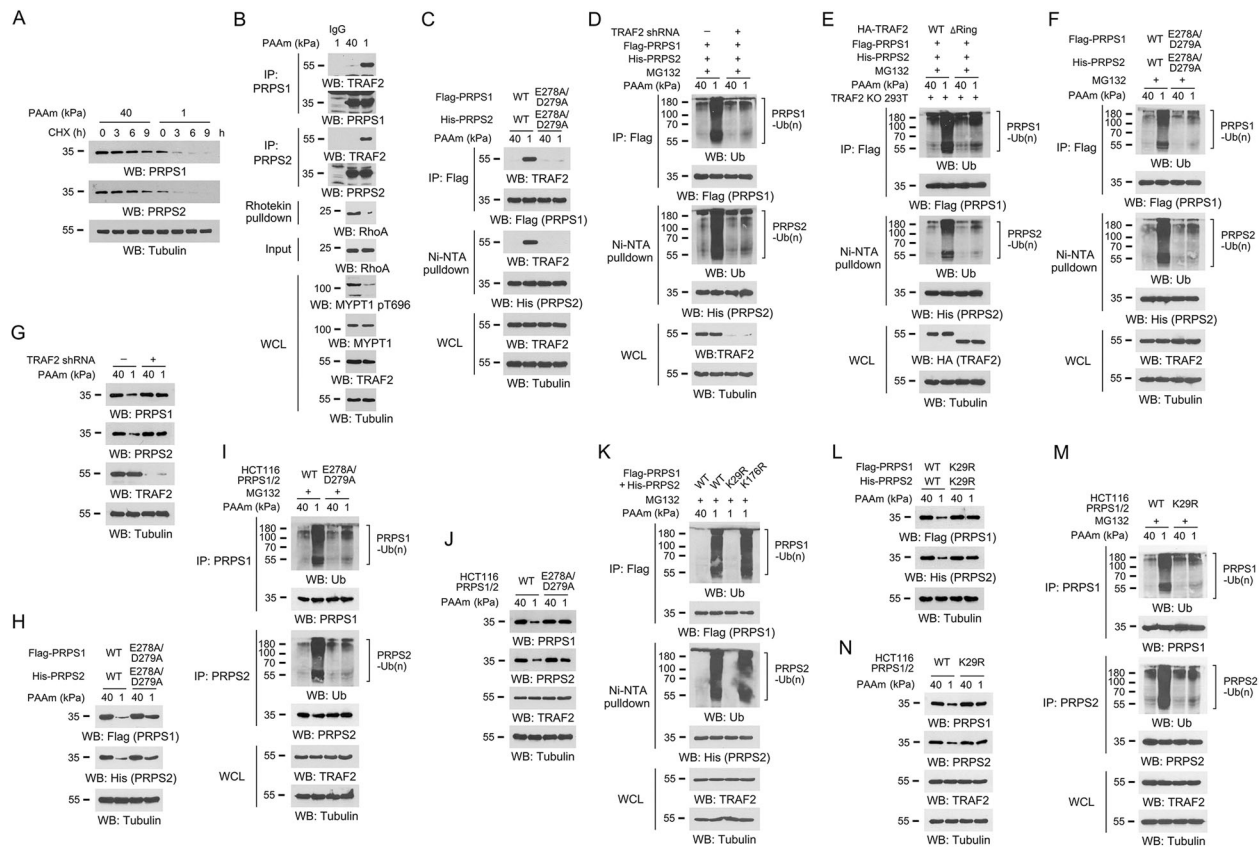


Fig. 2 TRAF2 mediates poly-ubiquitination and degradation of PRPS1/2 at low stiffness. **A–M** Cells were cultured on a stiff (40 kPa) or soft (1 kPa) PAAm matrix for 24 h before the indicated measurement or treatment. Immunoblot analyses were performed with the indicated antibodies. **A** HCT116 cells were treated with CHX (100 μg/ml) for the indicated periods of time. **B** Immunoprecipitation was performed using HCT116 cell lysates with the PRPS1 or PRPS2 antibodies. RhoA activity was examined. WCL, whole-cell lysate. **C** HCT116 cells were expressed with WT Flag-PRPS1, Flag-PRPS1 E278A/D279A, WT His-PRPS2, or His-PRPS2 E278A/D279A. Immunoprecipitation analyses with anti-Flag M2 agarose beads and Ni-NTA agarose bead pulldown were performed. **D** HCT116 cells with expression of TRAF2 shRNA, Flag-PRPS1, or His-PRPS2 were incubated with MG132 (10 μM) for 6 h. Immunoprecipitation analyses with anti-Flag M2 agarose beads and Ni-NTA agarose bead pulldown were performed. **E** TRAF2 KO HEK293T cells with expression of WT HA-TRAF2, HA-TRAF2 ΔRing, Flag-PRPS1, or His-PRPS2 were incubated with MG132 (10 μM) for 6 h. Immunoprecipitation analyses with anti-Flag M2 agarose beads and Ni-NTA agarose bead pulldown were performed. **F** HCT116 cells with expression of WT Flag-PRPS1, Flag-PRPS1 E278A/D279A, WT His-PRPS2 or His-PRPS2 E278A/D279A were incubated with MG132 (10 μM) for 6 h. Immunoprecipitation analyses with anti-Flag M2 agarose beads and Ni-NTA agarose bead pulldown were performed. **G** HCT116 cells were expressed with or without TRAF2 shRNA. **H** HCT116 cells were stably expressed with WT Flag-PRPS1, Flag-PRPS1 E278A/D279A, WT His-PRPS2, or His-PRPS2 E278A/D279A. **I** HCT116 cells with knock-in expression of PRPS1/2 E278A/D279A were incubated with MG132 (10 μM) for 6 h. Immunoprecipitation analyses were performed using indicated antibodies. **J** HCT116 cells were with a knock-in expression of PRPS1/2 E278A/D279A. **K** HCT116 cells with expression of WT Flag-PRPS1, Flag-PRPS1 K29R, Flag-PRPS1 K176R, WT His-PRPS2, His-PRPS2 K29R, or His-PRPS2 K176R were incubated with MG132 (10 μM) for 6 h. Immunoprecipitation analyses with anti-Flag M2 agarose beads and Ni-NTA agarose bead pulldown were performed. **L** HCT116 cells were stably expressed with WT Flag-PRPS1, Flag-PRPS1 K29R, WT His-PRPS2, or His-PRPS2 K29R. **M** HCT116 cells with knock-in expression of PRPS1/2 K29R were incubated with MG132 (10 μM) for 6 h. Immunoprecipitation analyses were performed using indicated antibodies. **N** HCT116 cells were with a knock-in expression of PRPS1/2 K29R.

Analysis of PRPS1/2 protein sequences revealed a shared and conserved four-residue motif₂₇₆PQED₂₇₉ (Fig. S2E), as an analog of the recognition consensus (P/S/A/T)x(Q/E)E for TRAF E3 ligases 1, 2, 3, and 5 [9]. The aspartic acid (D) at the C-termini of this motif possessed a negatively charged side chain, which is similar to glutamic acid (E) [10]. Immunoprecipitation analysis showed that soft matrix increased endogenous PRPS1/2 associated with TRAF2, rather than TRAFs 1, 3, or 5 (Figs. 2B and S2F, G). Further, disrupting this binding motif by mutation of E278/D279 into alanine (A) abrogated the association of endogenous TRAF2 with Flag-PRPS1 or His-PRPS2 (Fig. 2C).

We next examined whether TRAF2 was responsible for mechano-regulated PRPS1/2 ubiquitination. ShRNA-mediated knockdown of TRAF2 substantially blocked PRPS1/2 ubiquitination in HCT116 cells cultured on the soft matrix (Fig. 2D). Expression of a ring domain-truncated TRAF2 mutant [11], which lost its E3

ligase activity, failed to induce comparable PRPS1/2 ubiquitination in the endogenous TRAF2-depleted HEK293T cells (Fig. 2E). Similarly, PRPS1/2 E278A/D279A mutants showed an apparently reduced ubiquitination at low stiffness, compared to their wild-type (WT) counterparts (Fig. 2F). Consistently, knockdown of TRAF2 or mutation of TRAF2-binding motif rescued low stiffness-repressed PRPS1/2 expression in multiple cell lines (Figs. 2G, H and S2H). Further, double knock-in expression of PRPS1/2 E278A/D279A in HCT116 cells (Fig. S2I), by the CRISPR/Cas9 genome editing strategy, showed that mutated PRPS1/2 were less sensitive to be ubiquitinated (Fig. 2I), and were detected at comparable expression levels at low stiffness (Fig. 2J). These data suggest that TRAF2 mediates PRPS1/2 ubiquitination and degradation in response to low stiffness.

To identify the ubiquitylation site, we scanned PRPS1/2 protein sequences via the online prediction website UbPred

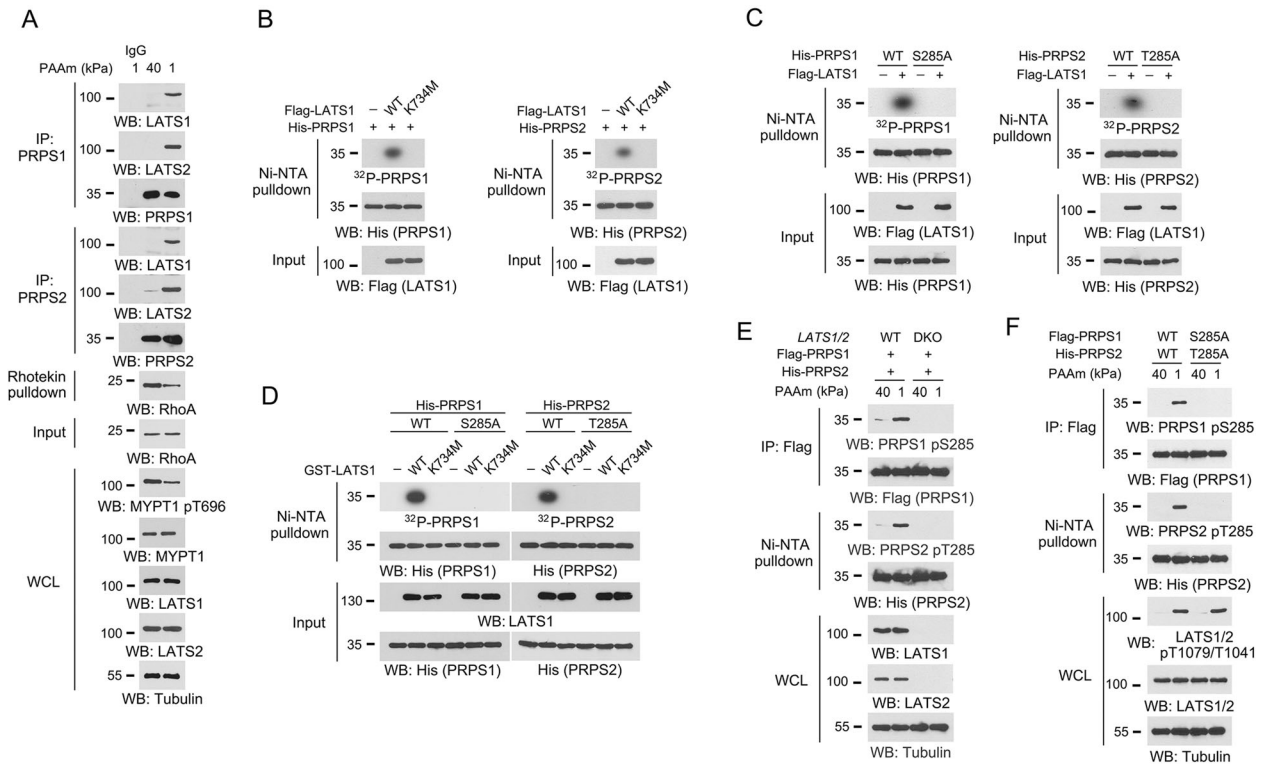


Fig. 3 LATS1/2 phosphorylate PRPS1 S285 and PRPS2 T285 at low stiffness. **A–F** Immunoblotting analyses were performed with the indicated antibodies. **A** HCT116 cells were cultured at indicated stiffness for 24 h. Immunoprecipitation was performed with the indicated antibodies. RhoA activity was examined. **B** Bacterially purified His-PRPS1 (left panel) or His-PRPS2 (right panel) protein was incubated with purified WT Flag-LATS1 or kinase-dead Flag-LATS1 K734M proteins in presence of $[\gamma\text{-}^{32}\text{P}]\text{-ATP}$ for an in vitro kinase assay. **C** Bacterially purified WT His-PRPS1, His-PRPS1 S285A (left panel), WT His-PRPS2 or His-PRPS2 T285A (right panel) protein was incubated with purified Flag-LATS1 protein in presence of $[\gamma\text{-}^{32}\text{P}]\text{-ATP}$ for an in vitro kinase assay. **D** Bacterially purified WT His-PRPS1, His-PRPS1 S285A, WT His-PRPS2, or His-PRPS2 T285A protein was incubated with bacterially purified WT GST-LATS1, GST-LATS1 K734M protein in presence of $[\gamma\text{-}^{32}\text{P}]\text{-ATP}$ for an in vitro kinase assay. **E, F** WT or LATS1/2 DKO MEFs (**E**), or HCT116 cells (**F**) with the expression of Flag-PRPS1 or His-PRPS2 were cultured at 40 kPa or 1 kPa for 24 h. Immunoprecipitation analyses with anti-Flag M2 agarose beads and Ni-NTA agarose bead pull-down were performed.

(<http://www.ubpred.org/>), and three lysine residues, K29, K110, and K176, that were shared by PRPS1/2, were found. Analysis of human PRPS1 structure (PDB code: 3EFH) revealed that K29 was exposed on the surface of PRPS1 hexamer, while K110 and K176 were localized in the interface between two units in the hexamer (Fig. S2J), where it was not likely to accommodate a poly-ubiquitin chain. Due to the high homology in the sequences of these two proteins, the spatial localization of these lysine residues in PRPS2 was supposed to be similar to that in PRPS1, though human PRPS2 structure was not available. Replacement of these lysines by arginine discovered that only mutation in K29, which is conserved among species (Fig. S2K), abolished soft matrix-induced PRPS1/2 ubiquitination (Fig. 2K). In line with this, compared to WT proteins, PRPS1/2 K29R mutants showed a higher expression level in HCT116, DU145, and HSC-3 cells cultured on the soft matrix (Figs. 2L and S2L). Further, knock-in of K29R mutation also blunted low stiffness-induced PRPS1/2 ubiquitination (Figs. 2M and S2M) and rescued PRPS1/2 expression (Fig. 2N). Such TRAF2-dependent mechanism was also observed between cells cultured on soft PAAm matrix and plastics (Fig. S3A–F). In addition, no obvious changes were found in the ubiquitination of the other two TRAF2 substrates MKP6 [12] and DYRK1A [13] (Fig. S3G), or the recruitment of TRAF2 in the lipid raft domain (Fig. S3H), where TRAF2 could be activated by TNF receptors [14], implying that the use of the soft and stiff hydrogels did not modulate the activity of TRAF2. Together, these results suggest that TRAF2 mediates the mechano-regulated ubiquitination of PRPS1/2 at K29 and subsequent degradation of PRPS1/2.

LATS1/2 phosphorylate PRPS1 S285 and PRPS2 T285 at low stiffness

We purified Flag-PRPS1 or His-PRPS2 protein from soft matrix-stimulated HCT116 cells and observed that treating these proteins with intestinal alkaline phosphatase (CIP) largely abolished their binding with bacterially purified GST-TRAF2 protein (Fig. S4A), implying that stiffness-responsive phosphorylation on PRPS1/2 was probably required for PRPS1/2 binding with TRAF2. To identify the potential kinase, Flag-PRPS1 protein was immunoprecipitated from the cell lysate of HCT116 cells cultured on soft matrix, and LATS2 was found in the PRPS1 immunoprecipitates by mass spectrometry analysis (Fig. S4B). Interaction of endogenous PRPS1/2 with LATS2 and its homolog kinase LATS1 was validated in HCT116 and HSC-3 cells (Figs. 3A and S4C). As a matter of course, TRAF2 was also identified in this proteomic screening (Fig. S4B).

LATS1/2 are serine/threonine protein kinases that play important roles in mechanoresponses [15]. At low stiffness, LATS1/2 were found to be active in HCT116, DU145, and HSC-3 cells, as shown by the markedly increased phosphorylation at LATS1 T1079 and LATS2 T1041 (Fig. S4D) [16]. An in vitro kinase assay revealed that phosphorylation of purified PRPS1 or PRPS2 proteins could be detected after incubation with WT LATS1 or LATS2 proteins purified from HEK293 cells, but not the kinase-dead LATS1 K734M or LATS2 K697A mutant (Figs. 3B and S4E). PRPS1 or PRPS2 proteins derived from the in vitro protein kinase assay were further examined by liquid chromatography-tandem mass spectrometry, which discovered phosphorylation on PRPS1 S285 and PRPS2 T285 (Fig. S4F). Both serine and threonine possess a polar

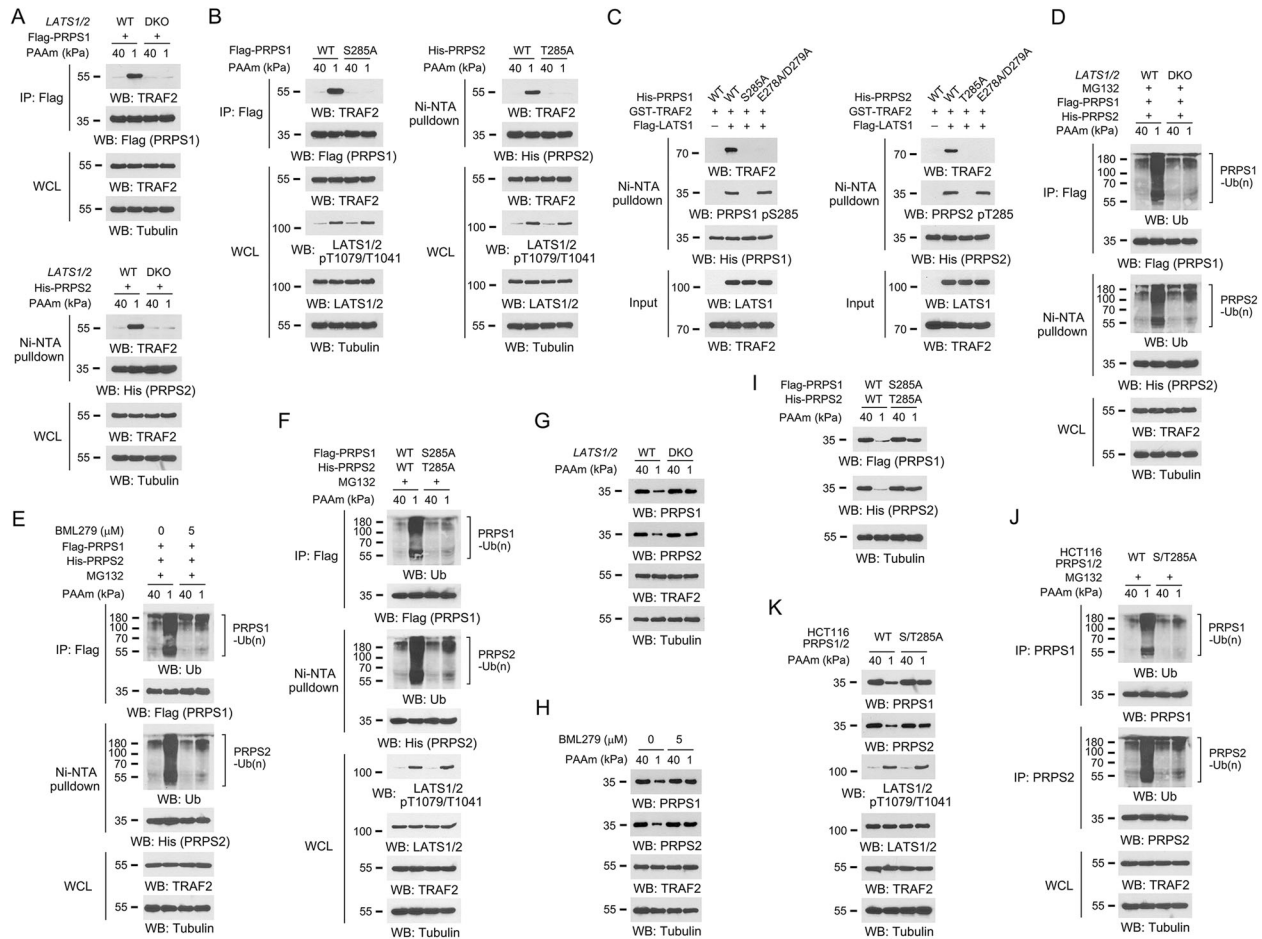


Fig. 4 LATS1/2-dependent S/T285 phosphorylation is required for PRPS1/2 ubiquitination and degradation at low stiffness. **A, B, D–K** Cells were cultured on a stiff (40 kPa) or soft (1 kPa) matrix for 24 h before indicated measurement or treatment. **A–K** Immunoblot analyses were performed with the indicated antibodies. **A** WT or LATS1/2 DKO MEFs were expressed with Flag-PRPS1 (upper panel) or His-PRPS2 (bottom panel). Immunoprecipitation analyses with anti-Flag M2 agarose beads or Ni-NTA agarose bead pulldown were performed. **B** HCT116 cells were expressed WT Flag-PRPS1, Flag-PRPS1 S285A (left panel), WT His-PRPS2, or His-PRPS2 T285A (right panel). Immunoprecipitation analyses with anti-Flag M2 agarose beads and Ni-NTA agarose bead pulldown were performed. **C** Bacterially purified WT His-PRPS1, His-PRPS1 S285A, His-PRPS1 E278A/D279A (left panel), WT His-PRPS2, His-PRPS2 T285A, or His-PRPS2 E278A/D279A (right panel) protein was incubated with purified Flag-LATS1 protein for an in vitro kinase assay. The PRPS1/2 proteins were pulldown, washed, incubated with bacterially purified TRAF2 proteins. A Ni-NTA agarose bead pulldown was performed. **D** WT or LATS1/2 DKO MEFs with an expression of Flag-PRPS1 or His-PRPS2 were incubated with MG132 (10 μM) for 6 h. Immunoprecipitation analyses with anti-Flag M2 agarose beads and Ni-NTA agarose bead pulldown were performed. **E** HCT116 cells were incubated with 5 μM BML279 in the presence of MG132 (10 μM) for 9 h. Immunoprecipitation analyses with anti-Flag M2 agarose beads and Ni-NTA agarose bead pulldown were performed. **F** HCT116 cells with expression of WT Flag-PRPS1, Flag-PRPS1 S285A, WT His-PRPS2, or His-PRPS2 T285A were incubated with MG132 (10 μM) for 6 h. Immunoprecipitation analyses with anti-Flag M2 agarose beads and Ni-NTA agarose bead pulldown were performed. **G** WT or LATS1/2 DKO MEFs were used. **H** HCT116 cells were incubated with 5 μM BML279 for 12 h. **I** HCT116 cells were stably expressed with WT Flag-PRPS1, Flag-PRPS1 S285A, WT His-PRPS2, or His-PRPS2 T285A. **J** HCT116 cells with knock-in expression of PRPS1/2 S/T285A were incubated with MG132 (10 μM) for 6 h. Immunoprecipitation analyses were performed with indicated antibodies. **K** HCT116 cells were with the knock-in expression of PRPS1/2 S/T285A.

phosphorylatable side chain, and alignment analysis revealed that the protein sequences flanking PRPS1/2 S/T285 were evolutionally conserved among species (Fig. S4G). Notably, replacement of PRPS1/2 S/T285 by alanine rescinded LATS1/2-mediated phosphorylation of PRPS1/2 (Figs. 3C and S4H). These observations were further confirmed by using bacterially purified GST-tagged LATS1 and LATS2 proteins (Figs. 3D and S4I). We then prepared antibodies specifically recognizing the phosphorylated PRPS1 S285 or PRPS2 T285, respectively (Fig. S4J), and found that double-knockout (DKO) of LATS1/2 in mouse embryonic fibroblasts (MEFs) (Figs. 3E and S4K) or expression of PRPS1 S285A and PRPS2 T285A (hereafter abbreviated as PRPS1/2 S/T285A) mutants in HCT116 cells (Fig. 3F) abrogated these phosphorylations. These results indicate that LATS1/2 phosphorylate PRPS1/2 S/T285 in response to low rigidity.

LATS1/2-dependent PRPS1/2 S/T285 phosphorylation is required for PRPS1/2 ubiquitination and degradation at low stiffness

PRPS1/2 S/T285 was close to TRAF2-binding motif P276/E278/D279 (Fig. S4G), hinting at a potential impact of this phosphorylation on the interaction between PRPS1/2 and TRAF2. We pulldown the Flag-PRPS1 or His-PRPS2 proteins from WT or LATS1/2 DKO MEFs, and found very few PRPS1/2-associated TRAF2 proteins at high stiffness, regardless of LATS1/2 expression. While, at low stiffness, loss of LATS1/2 markedly reduced the amount of TRAF2 protein detected in PRPS1/2 precipitates (Fig. 4A). In addition, non-phosphorylatable PRPS1/2 S/T285A mutants failed to pulldown a similar amount of TRAF2 protein at low stiffness compared to WT PRPS1/2, even in the presence of active LATS1/2 (Fig. 4B). Further, we incubated bacterially purified WT or mutant PRPS1/2

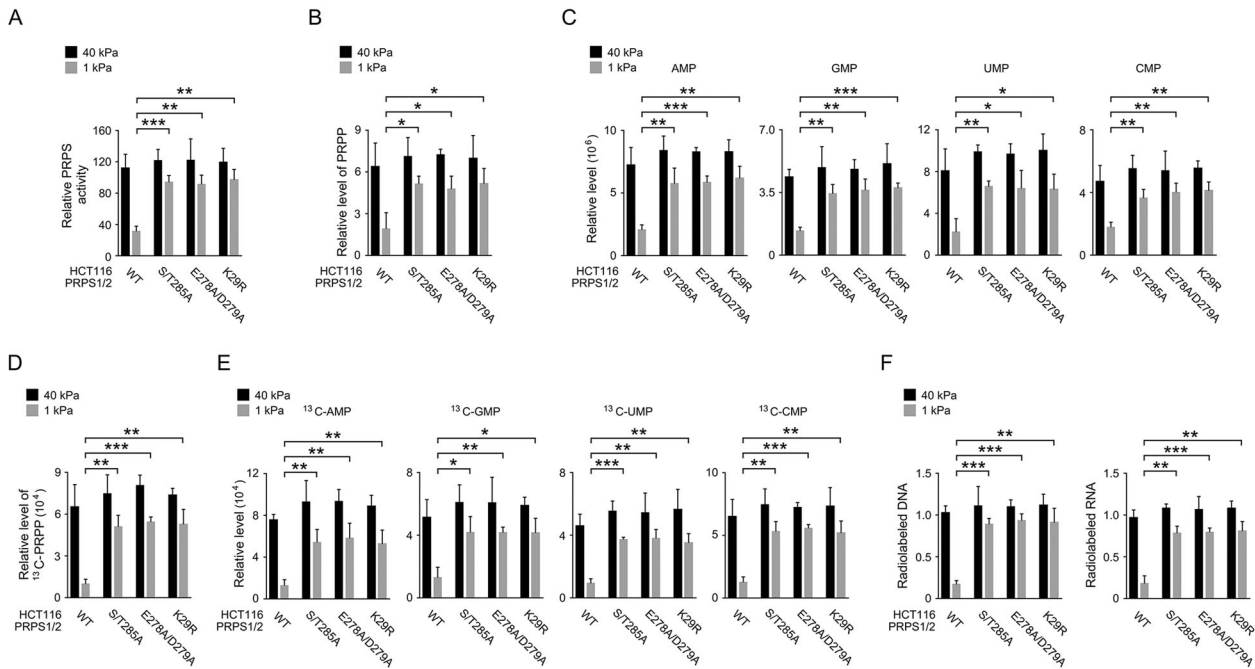


Fig. 5 PRPS1/2 S/T285 phosphorylation and K29 ubiquitination are required for low stiffness-repressed nucleotide synthesis. A–F Cells were cultured on a stiff (40 kPa) or soft (1 kPa) matrix for 24 h before indicated measurement or treatment. Data represent the mean and SD from three independent experiments. * $P < 0.05$, ** $P < 0.01$, *** $P < 0.001$. **A** PRPS activities in cell lysates from WT or indicated mutant HCT116 cells were examined. **B, C** Indicated metabolites in WT or indicated mutant HCT116 cells were measured. **D, E** WT or indicated mutant HCT116 cells were labeled with $^{13}\text{C}_6$ -glucose (10 mmol/L) for 2 h, and the indicated ^{13}C -labeled metabolites were measured. **F** WT or indicated mutant HCT116 cells were labeled with $^{14}\text{C}_6$ -glucose (1 μCi , 0.01 mmol/L) for 2 h, and the amounts of ^{14}C -DNA and ^{14}C -RNA were measured.

proteins with purified Flag-LATS1 protein for an in vitro kinase assay and measured the binding affinity of these PRPS1/2 proteins to purified GST-TRAF2 protein. This assay revealed that only phosphorylated WT PRPS1/2 proteins could efficiently associate with TRAF2 protein (Fig. 4C). These results suggest that LATS1/2-dependent S/T285 phosphorylation is required for PRPS1/2 binding to TRAF2.

Rho/ROCK operates through the Hippo pathway in response to extracellular signals [15, 17]. Indeed, when cultured on stiff matrix, treatment with Rho inhibitor Rhosin [18], ROCK inhibitor Y27632 [19], or non-muscle myosin inhibitor Blebbistatin [20] markedly induced S/T285 phosphorylation, TRAF2 interaction, and ubiquitination of PRPS1/2 in HCT116 (Fig. S5A–F). These effects were accompanied by the activation of LATS1/2, increased phosphorylation of YAP1 S127 and TAZ S89, and reduced expression of YAP1 and TAZ (Fig. S5A, C, F). Low ECM rigidity acts through phospholipase $\text{C}\gamma 1$ (PLC $\gamma 1$) and phospholipase D1/2 (PLD1/2) to accumulate phosphatidic acid on the cell membrane, which sequentially activates mammalian STE20-like kinases MST1/2 and LATS1/2 (Fig. S6A) [15]. In MST1/2-silenced HCT116 cells, soft matrix-induced LATS1/2 activation was largely abolished compared to MST1/2 intact cells (Fig. S6B). Accordingly, PRPS1/2 were barely phosphorylated at S/T285 and interacted with much less TRAF2 protein (Fig. S6B). Similar results were observed under BML279-mediated inhibition of PLD1/2 (Fig. S6C). Intriguingly, treatment with PLC $\gamma 1$ antagonist U73122, which enriched a GFP-tagged PtdIns(4,5)P2 reporter in the plasma membrane, induced PRPS1/2 phosphorylation and their binding with TRAF2 in HCT116 cells even at high stiffness (Fig. S6D, E).

In line with the aforementioned findings, either loss of LATS1/2, treatment of BML279, or expression of PRPS1/2 S/T285A mutants abrogated PRPS1/2 ubiquitination and restored PRPS1/2 expression in multiple cell lines cultured at soft matrix (Figs. 4D–I and

S6F). Similarly, CRISPR/Cas9 technology-introduced knock-in of S/T285A mutation rendered PRPS1/2 proteins resistant to low stiffness-induced ubiquitination and degradation (Figs. 4J, K and S6G–I). Together, these data suggested that LATS1/2-dependent S/T285 phosphorylation is a prerequisite for PRPS1/2 ubiquitination and degradation.

We further knockdown endogenous YAP1 and TAZ in HCT116 cells and stably expressed YAP1 5SA or TAZ 4SA mutants, whose LATS1/2 phosphorylation sites were replaced (YAP1: S61A, S109A, S127A, S164A, and S381A; TAZ: S66A, S89A, S117A, and S311A) [21, 22]. We found that these YAP1 and TAZ mutants were apparently more stable at low stiffness compared to their WT counterparts (Fig. S6J). Nevertheless, though the expression of YAP1 5SA and TAZ 4SA markedly restored the expression of their target gene CYR61, only limited effects were observed on PRPS1/2 binding to TRAF2, PRPS1/2 ubiquitination, or the cellular expression level of PRPS1/2 (Fig. S6J–L), suggesting that YAP1 or TAZ are not likely involved in mechanics-mediated regulation of PRPS1/2.

PRPS1/2 S/T285 phosphorylation and K29 ubiquitination is required for low stiffness-repressed nucleotide synthesis
At low stiffness, either knock-in expression of PRPS1/2 S/T285A, E278A/D279A, or K29R mutants in HCT116 cells or reconstituted expression of these mutants in endogenous PRPS1/2-silenced HSC-3 cells (Fig. S7A) substantially restored the cellular PRPS activity (Figs. 5A and S7B). Expression of these PRPS1/2 mutants augmented both the steady level and synthesis of PRPP and nucleotide intermediates (Figs. 5B–E and S7C–F). Consistently, more [^{14}C]-glucose-derived DNA or RNA were detected in PRPS1/2-mutated HCT116 or HSC-3 cells cultured on soft matrix, compared to their WT counterparts (Figs. 5F and S7G). These results suggest that PRPS1/2 S/T285 phosphorylation and K29 ubiquitination are required for matrix solidity-regulated nucleotide synthesis.

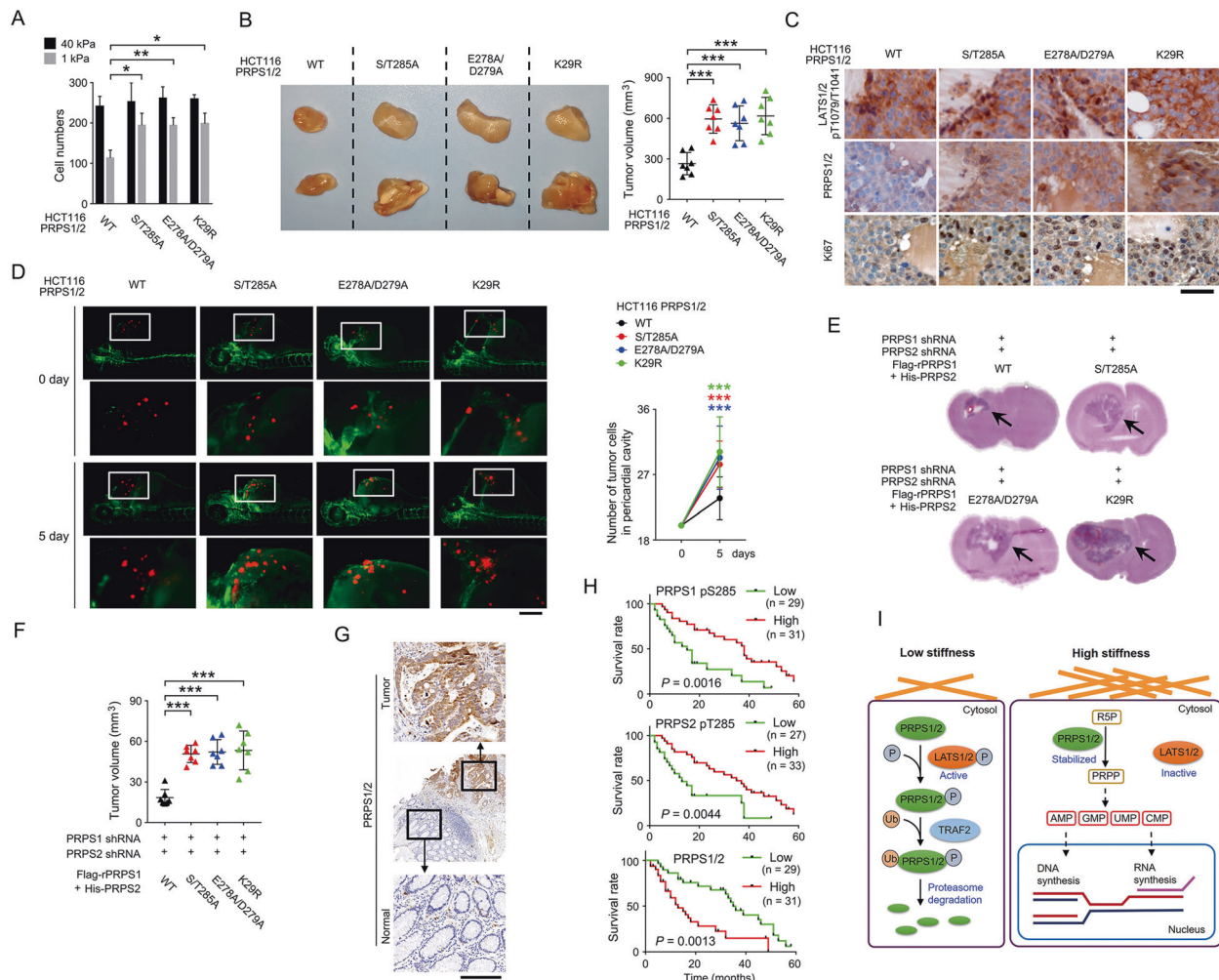


Fig. 6 Stabilized PRPS1/2 promotes tumorigenesis. **A** WT or the indicated mutant HCT116 cells were cultured at 40 or 1 kPa for 48 h. Cell numbers were counted. Data represent the mean and SD from three independent experiments. $*P < 0.05$, $***P < 0.01$. **B, C** WT or HCT116 cells with knock-in expression of the indicated mutants were subcutaneously injected in mice with soft hydrogel (0.60 ± 0.13 kPa). The volume of mice tumor xenografts ($n = 7$) was measured 21 days after injection. The images of two representative xenografts from each group were shown. Data represent the mean and SD. $***P < 0.001$ (**B**). Tumor tissues were analyzed by IHC staining with the indicated antibodies. Scale bar, $50 \mu\text{m}$ (**C**). **D** WT or HCT116 cells with knock-in expression of the indicated mutants were stained with CM-Dil Dye (red), suspended in 50% Matrigel (0.1 ± 0.022 kPa), and then microinjected into the pericardial cavity of Tg(flk1: EGFP) zebrafish (blood vessels labeled with GFP). The number of tumor cells in each group ($n = 15$) were counted immediately and 5 days after injection. The boxed areas were enlarged and shown underneath. Scale bar for original images, $300 \mu\text{m}$; for enlarging images, $100 \mu\text{m}$. Data represent the mean and SD. $***P < 0.001$. **E, F** Endogenous PRPS1/2-depleted HSC-3 cells with expression of WT Flag-rPRPS1, WT His-PRPS2, or indicated mutants were intracranially injected in mice ($n = 7$). Mice were sacrificed 21 days after injection and the tumor growth was analyzed by H&E staining (**E**). Tumor volume was measured (**F**). Data represent the mean and SD. $***P < 0.001$. **G** Expression of PRPS1/2 was examined in colorectal cancer tissues ($n = 60$) and non-cancerous adjacent tissues ($n = 60$). The boxed areas are enlarged. Scale bar for the original image, 1.5 mm; scale bar for enlarged images, $400 \mu\text{m}$. **H** Kaplan–Meier plots of the overall survival time of colorectal cancer patients ($n = 60$) with high or low expression of PRPS1 pS285, PRPS2 pT285, or PRPS1/2 were performed. P value was calculated using the log-rank test. **I** Model of LATS1/2 and TRAF2-governed PRPS1/2 stability and nucleotide metabolism in response to mechanical signals.

Stabilized PRPS1/2 promotes tumor cell proliferation and tumorigenesis

We next determined the impact of ECM rigidity-regulated PRPS1/2 stability on tumor cell proliferation. The shift from stiff to soft matrix impeded proliferation in both HCT116 and HSC-3 cells (Figs. 6A and S8A). Knock-in expression of PRPS1/2 S/T285A, E278A/D279A or K29R in HCT116 cells or reconstituted expression of these mutants in HSC-3 cells enhanced cell proliferation at low stiffness, but showed minor effects on those cells cultured on the stiff matrix (Figs. 6A and S8A), suggesting that disruption of PRPS1/2 degradation selectively regulated cell growth at low stiffness. In line with this, loss of LATS1/2 significantly restored the proliferation of HCT116 cells cultured on the soft matrix (Fig. S8B, C).

Further, WT HCT116 cells were mixed with a chondroitin sulfate-containing hydrogel and subcutaneously injected in mice, to recapitulate a soft (0.60 ± 0.13 kPa) or stiff (33 ± 2.73 kPa) tissue environment [23]. As expected, soft hydrogel palpably impeded tumor growth (Fig. S8D), with increased LATS1/2 T1079/1041 phosphorylation, declined MYPT1 T696 phosphorylation, and repressed PRPS1/2 and Ki67 expression (Fig. S8E). Notably, at low stiffness, HCT116 cells with S/T285A, E278A/D279A, or K29R mutations grew faster, and showed a higher PRPS1/2 and Ki67 expression, compared to WT cells (Fig. 6B, C). Accordingly, knockdown of LATS1/2 by distinct shRNAs also accelerated the formation of tumor xenografts (Fig. S8F).

We then microinjected the fluorescent dye-probed HCT116 cells, that were suspended in 50% Matrigel (0.1 ± 0.022 kPa) [24],

into the pericardial cavity of EGFP-labeled zebrafish embryos, so that in vivo tumor growth could be visualized (Fig. S8G) [25, 26]. As expected, despite a nearly equal number of HCT116 cells injected, much more PRPS1/2-mutated tumor cells were found in the pericardial cavity 5 days after injection, compared to WT cells (Fig. 6D).

Lung and brain, both of which are among the softest tissues for mammals [1], are documented as the distant metastatic sites for colorectal cancer and oral squamous cell carcinoma, respectively [27, 28]. To test the intracranial growth of oral squamous cell carcinoma cells, we injected HSC-3 cells into the mouse brain. We found that those cells with non-phosphorylatable or non-ubiquitinatable PRPS1/2 mutations resulted in significantly larger intracranial tumor xenografts (Fig. 6E, F). In line with this, injection of genetically engineered HCT116 cells through mouse caudal vein caused more metastatic nodules on lung surface (Fig. S8H). These data strongly suggest that stabilization of PRPS1/2 promotes tumor cell growth in a low-stiff environment.

PRPS1/2 S/T285 phosphorylation correlates with clinical aggressiveness of colorectal cancer

We next performed IHC analyses of clinical colorectal tumor tissues and found that PRPS1/2 was highly expressed in tumor tissues compared to non-cancerous adjacent tissues (Figs. 6G and S8I), which was consistent with the previous findings that tumor tissues are stiffer than non-tumorous normal tissues [1]. The IHC staining scores of PRPS1/2 S/T285 phosphorylation were positively correlated with LATS1/2 T1079/T1041 phosphorylation but negatively correlated with PRPS1/2 expression (Fig. S8J). In addition, those patients who had high phosphorylation of PRPS1/2 S/T285 or low expression of PRPS1/2 showed a longer survival duration (Fig. 6H). These results suggest a relationship between PRPS1/2 S/T285 phosphorylation and clinical aggressiveness of colorectal cancer.

DISCUSSION

A tumor-hosting environment elicits variable mechanical cues that establish complex interplay between cells and their surroundings [1]. It is documented that tumor niche stiffening induces glutaminase-dependent aspartate production, which in turn enhances the biosynthesis of purine and pyrimidine rings in tumor cells [29]. Nevertheless, it is still largely unclear how nucleotide metabolism is tuned with extracellular mechanical forces. In this study, we demonstrate that ECM stiffness regulates PRPP production, which is an upstream step prior to the formation of purine and pyrimidine rings during nucleotide synthesis. We found a repressed nucleotide synthesis in tumor cells at low ECM stiffness, as evidenced by the decreased steady level and synthesis of nucleotide intermediates, and the reduced amounts of glucose-derived DNA and RNA. Importantly, the shrunken nucleotide pool was caused by the impaired PRPP synthesis, since the metabolic flux from glucose to fructose-6-P and R5P stayed intact. It is reported that environmental stiffness modulated glycolytic rates in non-small-cell lung cancer cells [30]. Therefore, glycolysis, PPP pathway, and nucleotide synthesis are probably separately regulated in response to ECM rigidity in a cell type-dependent manner.

The hippo pathway is widely established as a crucial effector in mechanotransduction [1]. MST/LATS kinases, the core components of the Hippo pathway, reconcile the phosphorylation of transcriptional co-activators YAP1/TAZ to regulate tumor progression [31]. Consistently in this report, we demonstrate that culture on soft matrix evoked LATS1/2 activation, which could be abolished by modulating Rho/ROCK cascade, MST1/2, PLD1/2, or PLC γ 1. Of note, our data also show that activated LATS1/2 phosphorylated PRPS1/2 at S/T285, which primed PRPS1/2 binding with TRAF2,

leading to TRAF2-mediated K29 ubiquitination and degradation of PRPS1/2. This LATS1/2 and TRAF2-dependent mechanism rendered the stability of PRPS1/2 protein sensitive to mechanical signals and thereby coupled nucleotide metabolism to ECM rigidity. In addition, it is observed that mechanical cues modulated the expression of a couple of enzymes involved in deoxynucleotide synthesis, including ribonucleotide reductase subunits RRM1 and RRM2, thymidylate synthetase, deoxythymidylate kinase, and thymidine kinase, in a YPA/TAZ-dependent manner [32]. In the present data, however, stiffness regulated PRPS1/2 phosphorylation and ubiquitination regardless of the activation status of YAP1/TAZ. Therefore, it is likely that nucleotide metabolic enzymes are probably regulated in response to ECM remodeling through distinct mechanisms.

Loss of mechano-homeostasis is a hallmark of tumor development. In this study, our findings illustrate a novel and important role of environmental mechano-cues in the regulation of tumor cell metabolism. ECM rigidity signals govern nucleotide synthesis by modulating PRPS1/2 stability in a LATS1/2 and TRAF2-dependent manner (Fig. 6I). Disruption of this mechano-sensitive cascade boosts nucleotide synthesis and benefits tumor growth.

EXPERIMENTAL PROCEDURES

Materials

Rabbit polyclonal antibodies recognizing unmodified PRPS1, PRPS2, and phosphorylated PRPS1 S285 or phosphorylated PRPS2 T285 were customized from Boer Biotechnology (Chengdu, China). To prepare the PRPS1 antibody, a synthetic peptide (KWIRENISEWRNCT) was injected into rabbits. Rabbit serum was collected and purified using an affinity column conjugated with recombinant PRPS2 protein to exclude antibodies recognizing PRPS2, followed by an affinity column conjugated with recombinant PRPS1 protein to bind to and purify the antibody. The PRPS2 antibody was generated by using a peptide immunogen (QWIRENIAEWKNCI). To prepare antibody recognizing PRPS1 pS285 or PRPS2 pT285, peptides containing PRPS1 pS285 or PRPS2 pT285 were injected into rabbits. The rabbit serum was collected and purified using an affinity column conjugated with non-modified peptide to exclude the antibodies recognizing non-phosphorylated PRPS1/2, followed by an affinity column conjugated with PRPS1 pS285 or PRPS2 pT285 peptide to bind to and purify the antibodies. Antibodies were then eluted and concentrated.

Antibodies recognizing MST1 (#14946), MST2 (#3952), YAP1 (#12395), TAZ (#83669), TRAF2 (#4724), CYR61 (#14479), MYPT1 (#8574), MYPT1 pT696 (#5163), RhoA (#2117), CAV1 (#3238), DYRK1A (#8765) and ubiquitin (#3936) were obtained from Cell Signaling Technology. Antibody recognizing both PRPS1 and PRPS2 (sc-100822) was obtained from Santa Cruz. Antibody recognizing both LATS1 and LATS2 (BS-4081R) was obtained from Bioss. Antibodies recognizing Tubulin (ab7291), LATS1/2 pT1079/T1041 (ab111344), LATS1 (ab243656), LATS2 (ab243657), MKP6 (ab272587), Ki67 (ab16667), TRAF1 (ab252875), TRAF3 (ab239357), TRAF5 (ab137763), Flag (ab205606), GST (ab36415) and His (ab18184) were obtained from Abcam. Antibody against anti-Flag M2 agarose beads, streptavidin-conjugated agarose beads, Hoechst, ATP, and bovine serum albumin was purchased from Sigma. GFP-Trap beads were purchased from ChromoTek. BML279 was obtained from Abcam. Rhosin was obtained from R&D Systems. U73122, Y27632, Blebbistatin, MG132, and CHX were obtained from Sigma-Aldrich. Horseradish peroxidase-conjugated goat anti-mouse or rabbit secondary antibodies were obtained from Thermo Fisher Scientific. [γ - 32 P]-ATP was purchased from MP Biomedicals. [13 C $_6$]-glucose, [13 C $_2$, 15 N]-glycine, and [13 C $_5$, 15 N $_4$]-hypoxanthine were purchased from Cambridge Isotope Laboratories. Lipofectamine 2000 was obtained from Thermo Fisher Scientific.

DNA constructs and mutagenesis

PCR-amplified human Ub, PRPS1, PRPS2, TRAF2, YAP1, TAZ, LATS1, and LATS2 were subcloned into pcDNA3.1/hygro(+)-Flag, pcDNA3.1/hygro(+)-HA, pcDNA3.1/hygro(+)-Myc, pCDH-SFB, or pCold I (His) vectors. Mutants were constructed using the QuikChange site-directed mutagenesis kit (Stratagene, La Jolla, CA).

The following shRNAs were used: control shRNA, GCT TCT AAC ACC GGA GGT CTT; PRPS1 shRNA, GAT AAT ATG ATC TGC ACC T; PRPS2 shRNA, TAA ACC AAT ACA AGC ACT G (targeting non-coding region); YAP1 shRNA, ATA TAC AAC ACA GTG ATT G (targeting non-coding region); TAZ shRNA, CCT GCA TTT CTG TGG CAG ATA (targeting non-coding region); TRAF2 shRNA, AAC TCT GT CTT CGT GAG CT (targeting non-coding region); MST1 shRNA, TAT AAT TCC TTC CAG GAC C; MST2 shRNA, TTA ATT GCG ACA ACT TGA C; LATS1 shRNA-1, CAC GGC AAG ATA GCA TGG ATT; LATS1 shRNA-2, GAA GAT AAA GAC ACT AGG AAT; LATS2 shRNA-1, GCC ATG AAG ACC CTA AGG AAA; LATS2 shRNA-2, CCT CTG GGA TGA TGT GTC TAA.

shRNA-resistant rPRPS1 vectors were generated by introducing nonsense mutations of a568b, t571c, t574c, and t577c.

Cell culture

HCT116, DU145, and HEK293 cells were obtained from ATCC, and HSC-3 cells were obtained from JCRB Cell Bank. All the cell lines were authenticated and tested to confirm no mycoplasma contamination before use. All the cell lines were maintained with Dulbecco's Modified Eagle Medium supplemented with 10% fetal bovine serum. Cells with or without knock-in or exogenous expressions were cultured on the stiff or soft matrix for 24 h before indicated measurements or treatments.

For generating shRNA-depleted stable cell lines, cells were transfected with shRNA plasmids and selected by puromycin. For generating gene-expressing stable cell lines, shRNA-depleted cells were infected with lentivirus carrying WT or mutant gene and selected by hygromycin or/and G418.

Transfection of plasmids was performed by using Lipofectamine 2000, following the manufacture's instructions.

Preparation of cell culture matrix

For PAAm gel, acrylamide/bis-acrylamide (Bio-Rad, Hercules, CA) at final concentrations of 3/0.1 or 8/0.5 w/v% was used to create the soft (0.98 ± 0.029 kPa) or stiff (40.19 ± 3.19 kPa) PAAm gel, respectively [6, 7]. The gelation reaction was triggered by adding 10% ammonium persulfate and 1/1000 volume of N, N, N₀-tetramethylethylenediamine into acrylamide and bis-acrylamide Solutions (Fisher BioReagents). This solution was then sandwiched between the methacrylate-functionalized coverslip and a DCDMS-coated glass slide. After reacting for 30 min, the polyacrylamide gels were rinsed three times with PBS and allowed to hydrate in PBS overnight. Gels were then sterilized in a tissue culture hood by exposure to 254 nm, 30 W UV light for 4 h. For protein attachment, the surface of the PAAm gel was reacted with the photoactivated, bi-functional crosslinker Sulfosuccinimidyl 6-(4-azido-20-nitrophenylamino)hexanoate (sulfo-SANPAH, Pierce, 0.2 mg/mL in 50 mM HEPES pH 8.5) under 365 nm UV light with a surface intensity of 0.85 mW/cm² for 10 min. 10 µg/ml human placenta fibronectin (PureCol, Advanced BioMatrix) was used to coat the hydrogels or plastic tissue culture dishes, according to a previous report [15].

Cell proliferation assay

After indicated treatment, cell proliferation was evaluated by counting the number of cells.

Mass spectrometric analysis

Protein bands visualized via Coomassie Brilliant Blue staining were excised from SDS-PAGE gel and digested in 50 mM ammonium bicarbonate buffer containing RapiGest (Waters Corporation)

overnight at 37 °C with 200 ng of modified sequencing-grade trypsin (Promega). The digested samples were analyzed using high-sensitivity liquid chromatography-tandem mass spectrometry with an Orbitrap Elite mass spectrometer (Thermo Fisher Scientific). Proteins were identified by searching the fragment spectra against the Swiss-Prot protein database (EBI) using the Mascot search engine (version 2.3; Matrix Science) with the Proteome Discoverer software program (version 1.4; Thermo Fisher Scientific). The Mass spectrometric was deposited in Mendeley Data (<https://doi.org/10.17632/4pv52f45cy.1>).

ROCK activity assay

ROCK activity was measured by using the ROCK activity assay kit (Sigma-Aldrich) following the manufacture's instruction.

Genomic editing

Genomic mutations in HCT116 cells were created using the CRISPR/Cas9 system as described previously [33]. Single guide RNAs (sgRNAs) were designed to target the genomic areas adjacent to human PRSP1 or PRPS2 mutation sites. Annealed guide oligos containing overhangs were inserted into the high-fidelity PX458-HF vector (Addgene) digested with the BbsI restriction enzyme. In a 24-well plate, HCT116 cells at 60% confluence were co-transfected with a single-stranded donor oligonucleotide (20 pmoles) used as a template to introduce the mutations, a vector (0.5 µg) able to co-express a sgRNA targeting the PRSP1 or PRPS2 gene, and WT hSpCas9 tagged with a green fluorescent protein. 24 h after transfection, cells were trypsinized and diluted in a medium for single-cell seeding into a 96-well plate, and green fluorescent protein-positive cells were marked and subjected to genomic DNA extraction. Genotyping was performed by sequencing PCR products amplified from primers spanning the mutation area.

Immunoprecipitation and immunoblot analysis

Extraction of proteins from cultured cells was performed with a lysis buffer (50 mM Tris-HCl [pH 7.5], 0.1% SDS, 1% Triton X-100, 150 mM NaCl, 1 mM dithiothreitol, 0.5 mM EDTA, 100 µM PMSF, 100 µM leupeptin, 1 µM aprotinin, 100 µM sodium orthovanadate, 100 µM sodium pyrophosphate, and 1 mM sodium fluoride). Cell extracts were clarified by centrifugation at 13,400 g, and the supernatants were subjected to immunoprecipitation with the indicated antibodies. After overnight incubation at 4 °C, protein A or G agarose beads were added and incubated for another 3 h. Immunocomplexes were washed with lysis buffer three times and then subjected to immunoblot analyses.

Purification of recombinant proteins

Expression of Flag-PRPS1, His-PRPS1, His-PRPS2, GST-TRAF2, GST-LATS1, GST-LATS2, and mutant proteins was induced in bacteria, and these proteins were purified as described previously [33]. Briefly, BL21(DE3) cells expressing His-, or GST-tagged proteins were cultured in 250 ml of LB medium and treated with isopropyl β-D-1-thiogalactopyranoside (IPTG) for 16 h at 30 °C before lysis via sonication.

Flag-tagged LATS1 and LATS2 recombinant proteins were expressed in HEK293 cells. Briefly, a pcDNA3.1 plasmid (10 µg) expressing Flag-LATS1 or Flag-LATS2 recombinant proteins was transfected into HEK293 cells seeded in a 15 cm-diameter dish with the confluence of 70%. Forty-eight hours after transfection, the cells were harvested with a non-denaturing lysis buffer (20 mM Tris HCl pH 8.0, 137 mM NaCl, 1% NP-40).

For purification of His-tagged proteins, cell lysates were loaded onto a Ni-NTA column (GE Healthcare Life Sciences) followed by washing with five column volumes of 20 mM imidazole and subsequent elution with 250 mM imidazole.

For purification of Flag-tagged proteins, cell lysates were loaded onto a column containing Anti-Flag M2 agarose affinity gel

followed by washing with five column volumes of phosphate-buffered saline (PBS) and subsequent elution with 100 µg/ml Flag peptide.

For GST-tagged proteins, cell lysates were loaded onto a GSTrap HP column (GE Healthcare Life Sciences) followed by washing with five column volumes of PBS and subsequent elution with 10 mM reduced glutathione.

The proteins were then loaded onto a HiPrep 16/60 Sephacryl S-200 HR gel filtration column (GE Healthcare Life Sciences) to remove contaminated proteins. The purification efficiency was examined using SDS-PAGE and colloidal Coomassie Brilliant Blue (G-250) staining.

RT-PCR

Total RNA was extracted using TRIzol reagent (Invitrogen) according to the manufacturer's instructions. A cDNA library was generated by reverse-transcribing 1 µg of RNA using an iScript cDNA synthesis kit (Bio-Rad) and then amplified with primers recognizing the inconsonant part of PRPS1/2 mRNA, as follows: PRPS1-F: CCA CCA GGA CTT ATC TCA GAA AAT T; PRPS1-R: TGC AGT AAC CCG GCT GGC; PRPS2-F: GAC CTG TCC CAG CGC GTG; PRPS2-R: GAT CAC GGC AGT TAC TCT GGA TGA. The PCR products were examined via 1.5% agarose gel.

Measurement of endogenous PRPS Activity

Endogenous PRPS activity was measured following previous reports [34]. Briefly, 1×10^7 cells were quickly washed and homogenized in 1 ml reaction buffer on ice. 100 µl of cell lysates were supplemented with 4.7 mmol/l R5P, 3.2 mmol/l ATP and 20 µCi [γ - 32 P]ATP and incubated at 25 °C for 30 min. In total, 10 µl reaction sample was mixed with 5 µl 0.33 M formic acid and applied to PEI sheets. The sheets were chromatographed in 0.85 M potassium phosphate, pH 3.4, and autoradiographed. The radioactivity in the PRPP spots was determined by liquid scintillation counting.

Ubiquitination assay

Ubiquitination assay was performed following the previous report [35]. Cells were lysed using the denatured buffer (6 M guanidine-HCl [pH 8.0], 0.1 M Na₂HPO₄/NaH₂PO₄, and 10 mM imidazole) containing 5 mM N-ethylmaleimide to prevent deubiquitylation. The cell lysates were immunoprecipitated using the indicated antibodies, washed, and subjected to immunoblotting analysis.

In vitro LATS1/2 kinase assay

In vitro LATS1/2 kinase assay was performed following previous report [36]. The purified LATS1, LATS2, or mutant proteins (20 ng) were incubated with 100 ng purified PRPS1 or PRPS2 proteins in kinase buffer (30 mM HEPES, 50 mM potassium acetate, 5 mM MgCl₂, 500 µM ATP) in the presence or absence of 10 µCi [γ - 32 P]ATP for 30 min at 30 °C. The reaction was stopped by adding an SDS sample buffer. The protein samples were separated by SDS-PAGE and were detected by immunoblotting with indicated antibodies or by autoradiography.

The influx of [14 C]-labeled into DNA and RNA

The influx of [14 C]-glucose to DNA and RNA was performed as described previously [37]. In brief, cells were incubated with a medium containing 1 µCi of D-[6- 14 C] glucose (0.01 mmol/L) for the indicated time, followed by washing with PBS. RNA or DNA was extracted, and [14 C]-labeled RNA or DNA was quantified using a scintillation counter. The intensity of [14 C]-labeled RNA or DNA was normalized to total RNA or DNA.

Analysis of intermediate metabolites by LC/MS-MS

Metabolites were analyzed by high-resolution mass spectrometry (HRMS). For the cell sample, 5×10^7 cells were quickly washed with ice-cold PBS to remove extra-medium components. Nucleotide

metabolites were extracted using 90/9/1 (v/v/v) acetonitrile/water/formic acid, and PRPP were extracted by 75/25 (v/v) ethanol/10 mmol/l HEPES buffer. Samples were centrifuged at 17,000g for 5 min at 4 °C, and supernatants were transferred to clean tubes, followed by evaporation to dryness using nitrogen. Samples were reconstituted in 0.2% ammonium hydroxide in ammonium acetate (10 mmol/l), then 10 µl was injected into a Thermo Scientific Vanquish liquid chromatography system containing a Thermo Hypercarb HPLC column with mobile phase A (MPA) consisting of 0.2% ammonium hydroxide in ammonium acetate (10 mmol/L) and mobile phase B (MPB) consisting of 0.2% ammonium hydroxide in acetonitrile. Using a flow rate of 0.3 mL/min, the gradient elution program was: 0 min (0% MPB)–2.0 min (0% MPB)–15.0 min (30% MPB)–15.1 min (95% MPB)–20.0 min (95% MPB)–20.1 min (0% MPB)–25.0 min (STOP). Data were acquired using a Thermo Orbitrap Fusion Tribrid Mass Spectrometer via Selected Ion Mode (SIM) electrospray positive mode. Peak integration and area calculation were performed by using Thermo TraceFinder software.

For tracing metabolic flux, cells were incubated with [13 C₆]-glucose (10 mmol/l), [13 C₂, 15 N]-glycine (0.4 mmol/l) or [13 C₅, 15 N₄]-hypoxanthine (0.1 mmol/l) for indicated time. The metabolites were analyzed by HRMS with similar protocol.

Measurement of intracellular R5P Levels

The intracellular concentration of R5P was measured by using previously described methods, with some minor modifications [38]. In brief, 1×10^7 cells were washed, homogenized, centrifuged at 15,000 g for 10 min, and the supernatants were deproteinized using 10 kDa spin columns (EMD Millipore). The flow-through was mixed with 2× reaction buffer (100 mmol/l Tris-HCl [pH 8.0], 3.4 mmol/l ribulose-5-P, 0.004% w/v thiamine pyrophosphate, 30 mmol/l MgCl₂, 0.4 mmol/l NADH, 1 U α-glycerophosphate dehydrogenase, 10 U triosephosphate isomerase, and 1 U transketolase). The reaction was initiated by adding D-ribulose-5-phosphate 3-epimerase (0.5 U) and incubated at 25 °C for 30 min. The absorbance was read at 340 nm using a multi-detection microplate reader.

Rho activation assay

Rho activation assay was performed by using Active Rho Detection Kit #8820 (Cell Signaling Technology) following the manufacturer's instruction.

Lipid raft fraction preparation

Lipid raft fraction was prepared by using Minute™ Plasma Membrane-Derived Lipid Raft Isolation Kit (Invent Biotechnologies, Inc.) following the manufacturer's instruction.

Mice subcutaneous tumor model

Chondroitin sulfate methacrylate was synthesized following a previously reported method [39]. Briefly, chondroitin sulfate sodium salt was reacted with N-hydroxysuccinimide (NHS), and 1-ethyl-3-(3-dimethylaminopropyl)-carbodiimide (EDC) in 50 mM 2-morpholinoethanesulfonic acid (containing 0.5 M NaCl, pH 6.5) for 5 min before 2-aminoethyl methacrylate (AEMA) was added. NHS, EDC, and AEMA were reacted at a molar ratio of 1:2:1 for 24 h at room temperature, and were then dialyzed against water for 4 days, lyophilized, and stored at –20 °C.

Poly(ethylene glycol) dimethacrylate (MW 4.6 kDa) was dissolved in chondrogenic media to achieve final concentrations of 8% or 14% (w/v) for soft (0.60 ± 0.13 kPa) or stiff (33 ± 2.73 kPa) matrixes, respectively [23]. Cells were added to the hydrogel precursor solution, and the mixture was exposed to UV light (365 nm) for 3 min at 4 mW/cm² for photocrosslinking in presence of 0.05% (w/v) Lithium phenyl-2,4,6-trimethylbenzoylphosphinate. In total, 100 µL cell-hydrogel mixture containing 1×10^6 WT or mutant cells was subcutaneously implanted into 6-week-old

female BALB/c nude mice. Mice were sacrificed 21 days after implantation, and the tumor volume was calculated by the formula: $0.5 \times \text{length} \times \text{width}$ [2].

Mice intracranial tumor model

In total, 2×10^5 tumor cells suspended in 5 μl of DMEM medium were intracranially injected into 6-week-old female BALB/c nude mice, as described previously [35]. The mice were sacrificed 21 days after injection, and brain tissues were harvested, fixed in 4% formaldehyde, embedded in paraffin, sectioned, and subjected to H&E staining. Tumor volumes were calculated by the formula: $0.5 \times \text{length} \times \text{width}$ [2].

Mice lung tumor model

For the lung metastasis model, 5×10^4 WT or mutant HCT116 cells were injected into 6-week-old female BALB/c nude mice ($n = 7$) through the tail vein. Animals were sacrificed 14 days after injection and lungs were excised.

Zebrafish xenograft model

Zebrafish xenograft was established using Tg(flk1: EGFP) zebrafish following a previous report [40]. WT or mutant HCT116 cells were labeled with 2 μM CellTracker™ CM-Dil Dye (Thermo Fisher Scientific), washed with PBS, and then suspended in 50% Matrigel (0.1 ± 0.022 kPa) [24], and loaded onto a borosilicate glass needle pulled by a Flaming/Brown micropipette puller (Narishige, Japan, PN-30). Zebrafish embryos, 48 h postfertilization, were anesthetized by 0.003% tricaine. In total, 20 nL suspensions containing about 20 cells was implanted into the pericardial cavity of zebrafish embryo by using an electronically regulated air-pressure microinjector (Harvard Apparatus, NY, PL1-90). After injection, digital micrographs were taken with a Zeiss Imager. Z1 fluorescence microscope (Carl Zeiss Microimaging Inc., Germany) equipped with an AxioCam MRc5 digital CCD camera (Carl Zeiss Microimaging Inc., Germany). The number of CM-Dil-labeled tumor cells was evaluated through automated cell counting by using a custom Fiji (ImageJ2) software package [41, 42]. Those zebrafish embryos with 20 tumor cells were selected for each group ($n = 15$). Zebrafish were bred and maintained normally at 28 °C, pH 7.2–7.4. The CM-Dil-labeled tumor cells were quantified again 5 days after infection.

Clinical samples and immunohistochemical staining

The immunohistochemical staining was performed using the VECTASTAIN ABC kit (VECTOR LABORATORIES, CA) according to the manufacturer's instructions. Slides were quantitatively scored by 2 pathologists according to the percentage of positive cells and staining intensity, as previously defined [43]. We assigned the following proportion scores: 0 if 0% of the tumor cells showed positive staining, 1 if 0–10%, 2 if 11–30%, 3 if 31–70%, and 4 if 71–100%. We also rated the intensity of staining on a scale of 0 to 4: 0, negative; 1, weak; 2, moderate; 3, strong; 4, very strong. We then multiply the proportion and intensity scores to obtain a total score, which could be 10 distinct theoretical integer scores: 0, 1, 2, 3, 4, 6, 8, 9, 12, 16. The samples with the 5 lower scores were defined as low expression, while the samples with the 5 higher scores were defined as high expression. A total of 60 paired colorectal cancer tissues and non-cancerous adjacent normal tissues were obtained with informed consent from all subjects.

Quantification and statistical analysis

The sample size was determined to be adequate based on the magnitude and consistency of measurable differences between groups in all experiments in this study. No randomization was done, and no sample was excluded from the analyses. The investigators were blinded to patient information during scoring the IHC staining, while no blinding was used for other

experiments. Statistical analyses were conducted using two-sided Student's *t* test or ANOVA test. All data represent the mean \pm SD of at least three independent experiments/samples unless otherwise specified. Differences in means were considered statistically significant at $P < 0.05$. For every figure, statistical tests are justified as appropriate and the data met the assumptions of the tests. Finally, the variance between groups that were being statistically compared was similar.

DATA AVAILABILITY

All the data in this study is available in Figs. 1–6 and Supplementary Figs. S1–S8.

REFERENCES

- Butcher DT, Alliston T, Weaver VM. A tense situation: forcing tumour progression. *Nat Rev Cancer*. 2009;9:108–22.
- Discher DE, Janmey P, Wang YL. Tissue cells feel and respond to the stiffness of their substrate. *Science*. 2005;310:1139–43.
- Patra KC, Hay N. The pentose phosphate pathway and cancer. *Trends Biochem Sci*. 2014;39:347–54.
- Hove-Jensen B. Mutation in the phosphoribosylpyrophosphate synthetase gene (prs) that results in simultaneous requirements for purine and pyrimidine nucleosides, nicotinamide nucleotide, histidine, and tryptophan in *Escherichia coli*. *J Bacteriol*. 1988;170:1148–52.
- Nosal JM, Switzer RL, Becker MA. Overexpression, purification, and characterization of recombinant human 5-phosphoribosyl-1-pyrophosphate synthetase isozymes I and II. *J Biol Chem*. 1993;268:10168–75.
- Kwon HJ, Yasuda K. Chondrogenesis on sulfonate-coated hydrogels is regulated by their mechanical properties. *J Mech Behav Biomed Mater*. 2013;17:337–46.
- Young DA, Choi YS, Engler AJ, Christman KL. Stimulation of adipogenesis of adult adipose-derived stem cells using substrates that mimic the stiffness of adipose tissue. *Biomaterials*. 2013;34:8581–8.
- Khasnis M, Nakatomi A, Gumper K, Eto M. Reconstituted human myosin light chain phosphatase reveals distinct roles of two inhibitory phosphorylation sites of the regulatory subunit, MYPT1. *Biochemistry*. 2014;53:2701–9.
- Ye H, Park YC, Kreishman M, Kieff E, Wu H. The structural basis for the recognition of diverse receptor sequences by TRAF2. *Mol Cell*. 1999;4:321–30.
- Wang RW, Newton DJ, Huskey SE, McKeever BM, Pickett CB, Lu AY. Site-directed mutagenesis of glutathione S-transferase YaYa. Important roles of tyrosine 9 and aspartic acid 101 in catalysis. *J Biol Chem*. 1992;267:19866–71.
- Yin Q, Lamothe B, Darnay BG, Wu H. Structural basis for the lack of E2 interaction in the RING domain of TRAF2. *Biochemistry*. 2009;48:10558–67.
- Yang CY, Chiu LL, Tan TH. TRAF2-mediated Lys63-linked ubiquitination of DUSP14/MKP6 is essential for its phosphatase activity. *Cell Signal*. 2016;28:145–51.
- Zhang P, Zhang Z, Fu Y, Zhang Y, Washburn MP, Florens L, et al. K63-linked ubiquitination of DYRK1A by TRAF2 alleviates Sprouty 2-mediated degradation of EGRF. *Cell death Dis*. 2021;12:608.
- Legler DF, Micheau O, Doucey MA, Tschopp J, Bron C. Recruitment of TNF receptor 1 to lipid rafts is essential for TNF α -mediated NF- κ B activation. *Immunity*. 2003;18:655–64.
- Meng Z, Qiu Y, Lin KC, Kumar A, Placone JK, Fang C, et al. RAP2 mediates mechanoresponses of the Hippo pathway. *Nature*. 2018;560:655–60.
- Kim CL, Choi SH, Mo JS. Role of the hippo pathway in fibrosis and cancer. *Cells*. 2019;8.
- Rausch V, Hansen CG. The hippo pathway, YAP/TAZ, and the plasma membrane. *Trends Cell Biol*. 2020;30:32–48.
- Zhang Y, Duan X, Cao R, Liu HL, Cui XS, Kim NH, et al. Small GTPase RhoA regulates cytoskeleton dynamics during porcine oocyte maturation and early embryo development. *Cell Cycle*. 2014;13:3390–403.
- Chen Y, Wang D, Guo Z, Zhao J, Wu B, Deng H, et al. Rho kinase phosphorylation promotes ezrin-mediated metastasis in hepatocellular carcinoma. *Cancer Res*. 2011;71:1721–9.
- Lordier L, Bluteau D, Jalil A, Legrand C, Pan J, Rameau P, et al. RUNX1-induced silencing of non-muscle myosin heavy chain IIB contributes to megakaryocyte polyploidization. *Nat Commun*. 2012;3:717.
- Morishita T, Park HW, Qin B, Chen Q, Meng Z, Plouffe SW, et al. A YAP/TAZ-induced feedback mechanism regulates Hippo pathway homeostasis. *Genes Dev*. 2015;29:1271–84.
- Lei QY, Zhang H, Zhao B, Zha ZY, Bai F, Pei XH, et al. TAZ promotes cell proliferation and epithelial-mesenchymal transition and is inhibited by the hippo pathway. *Mol Cell Biol*. 2008;28:2426–36.

23. Wang T, Lai JH, Yang F. Effects of hydrogel stiffness and extracellular compositions on modulating cartilage regeneration by mixed populations of stem cells and chondrocytes in vivo. *Tissue Eng A*. 2016;22:1348–56.
24. Zaman MH, Trapani LM, Sieminski AL, Mackellar D, Gong H, Kamm RD, et al. Migration of tumor cells in 3D matrices is governed by matrix stiffness along with cell-matrix adhesion and proteolysis. *Proc Natl Acad Sci USA*. 2006;103:10889–94.
25. Zhao C, Wang X, Zhao Y, Li Z, Lin S, Wei Y, et al. A novel xenograft model in zebrafish for high-resolution investigating dynamics of neovascularization in tumors. *PLoS ONE*. 2011;6:e21768.
26. Nicoli S, Presta M. The zebrafish/tumor xenograft angiogenesis assay. *Nat Protoc*. 2007;2:2918–23.
27. Mitry E, Guiu B, Coscinea S, Jooste V, Faivre J, Bouvier AM. Epidemiology, management and prognosis of colorectal cancer with lung metastases: a 30-year population-based study. *Gut*. 2010;59:1383–8.
28. Liu JC, Bhayani M, Kuchta K, Galloway T, Fundakowski C. Patterns of distant metastasis in head and neck cancer at presentation: Implications for initial evaluation. *Oral Oncol*. 2019;88:131–6.
29. Bertero T, Oldham WM, Grasset EM, Bourget I, Boulter E, Pisano S, et al. Tumorstroma mechanics coordinate amino acid availability to sustain tumor growth and malignancy. *Cell Metab*. 2019;29:124–110.
30. Park JS, Burckhardt CJ, Lazzano R, Solis LM, Isogai T, Li L, et al. Mechanical regulation of glycolysis via cytoskeleton architecture. *Nature*. 2020;578:621–6.
31. Meng Z, Moroishi T, Guan KL. Mechanisms of Hippo pathway regulation. *Genes Dev*. 2016;30:1–17.
32. Santinon G, Brian I, Pocater A, Romani P, Franzolin E, Rampazzo C, et al. dNTP metabolism links mechanical cues and YAP/TAZ to cell growth and oncogene-induced senescence. *EMBO J*. 2018;37.
33. Li X, Jiang Y, Meisenhelder J, Yang W, Hawke DH, Zheng Y, et al. Mitochondria-translocated PGK1 functions as a protein kinase to coordinate glycolysis and the TCA cycle in tumorigenesis. *Mol Cell*. 2016;61:705–19.
34. Jensen KF, Houlberg U, Nygaard P. Thin-layer chromatographic methods to isolate 32P-labeled 5-phosphoribosyl-alpha-1-pyrophosphate (PRPP): determination of cellular PRPP pools and assay of PRPP synthetase activity. *Anal Biochem*. 1979;98:254–63.
35. Lee JH, Liu R, Li J, Zhang C, Wang Y, Cai Q, et al. Stabilization of phosphofructokinase 1 platelet isoform by AKT promotes tumorigenesis. *Nat Commun*. 2017;8:949.
36. Zhao B, Wei X, Li W, Udan RS, Yang Q, Kim J, et al. Inactivation of YAP oncoprotein by the Hippo pathway is involved in cell contact inhibition and tissue growth control. *Genes Dev*. 2007;21:2747–61.
37. Li X, Qian X, Peng LX, Jiang Y, Hawke DH, Zheng Y, et al. A splicing switch from ketohexokinase-C to ketohexokinase-A drives hepatocellular carcinoma formation. *Nat Cell Biol*. 2016;18:561–71.
38. Lin R, Elf S, Shan C, Kang HB, Ji Q, Zhou L, et al. 6-Phosphogluconate dehydrogenase links oxidative PPP, lipogenesis and tumour growth by inhibiting LKB1-AMPK signalling. *Nat Cell Biol*. 2015;17:1484–96.
39. Jeon O, Bouhadir KH, Mansour JM, Alsberg E. Photocrosslinked alginate hydrogels with tunable biodegradation rates and mechanical properties. *Biomaterials*. 2009;30:2724–34.
40. Zhao C, Yang H, Shi H, Wang X, Chen X, Yuan Y, et al. Distinct contributions of angiogenesis and vascular co-option during the initiation of primary microtumors and micrometastases. *Carcinogenesis*. 2011;32:1143–50.
41. Teng Y, Xie X, Walker S, White DT, Mumm JS, Cowell JK. Evaluating human cancer cell metastasis in zebrafish. *BMC Cancer*. 2013;13:453.
42. Schindelin J, Arganda-Carreras I, Frise E, Kaynig V, Longair M, Pietzsch T, et al. Fiji: an open-source platform for biological-image analysis. *Nat Methods*. 2012;9:676–82.
43. Lee JH, Liu R, Li J, Wang Y, Tan L, Li XJ, et al. EGFR-phosphorylated platelet isoform of phosphofructokinase 1 promotes PI3K activation. *Mol Cell*. 2018;70:197–210.e197.

ACKNOWLEDGEMENTS

We appreciate Mr. Mi Li at the University of Texas for proofreading.

AUTHOR CONTRIBUTIONS

RL conceived and designed the study; JL, JS, ZC, YH, CT, SHP, and J-HL performed the experiments; and RL wrote the paper with comments with all authors.

FUNDING

This work was supported by National Natural Science Foundation of China grants 81872218 (RL), 81772692 (JL); Scientific Research Program for Young Talents of China National Nuclear Corporation 2020CNNC74 (JL); the Science & Technology Department of Sichuan Province 2019YJ0371 (JL); Research Funding from West China School/Hospital of Stomatology Sichuan University (No. RCDWJS2020-8, RL) and Research Funding from West China School/Hospital of Chengdu Medical College (CYTD18-02, JL) and the National Research Foundation of Korea (NRF) grant funded by the Korea government (MSIT) 2020R1C1C1011350 (J-HL).

COMPETING INTERESTS

The authors declare no competing interests.

ETHICS STATEMENT

The use of human specimens and the database was approved by the Institutional Review Board at Chengdu Medical college (KJ2021015). The use of animals was approved by the Animal Care and Use Committee of West China Hospital of Stomatology (WCHSIRB-D-2019-142), and the animals were treated in accordance with relevant institutional and national guidelines and regulations.

ADDITIONAL INFORMATION

Supplementary information The online version contains supplementary material available at <https://doi.org/10.1038/s41418-021-00851-7>.

Correspondence and requests for materials should be addressed to R.L.

Reprints and permission information is available at <http://www.nature.com/reprints>

Publisher's note Springer Nature remains neutral with regard to jurisdictional claims in published maps and institutional affiliations.